Sciascera, C. and Giangrande, Paolo and Papini, Luca and Gerada, C. and Galea, Michael (2017) Analytical thermal model for fast stator winding temperature prediction. IEEE Transactions on Industrial Electronics, 64 (8). pp. 6116-6126. ISSN 0278-0046

Analytical Thermal Model for Fast Stator Winding Temperature Prediction

Claudio Sciascera, Paolo Giangrande, *Member, IEEE*, Luca Papini, Chris Gerada, *Senior Member, IEEE*, and Michael Galea, *Member, IEEE*

***Abstract*— This paper introduces an innovative thermal modelling technique which accurately predicts the winding temperature of electrical machines, both at transient and steady state conditions, for applications where the stator Joule losses are the dominant heat source. The model is an advanced variation of the classical Lumped Parameter Thermal Network approach, with the expected degree of accuracy but at a much lower computational cost. A 7-node Thermal Network is first implemented and an empirical procedure to fine-tuning the critical parameters is proposed. The derivation of the low computational cost model from the Thermal Network is thoroughly explained. A simplification of the 7-node Thermal Network with an equivalent 3-node Thermal Network is then implemented, and the same procedure is applied to the new network for deriving an even faster low computational cost model. The proposed model is then validated against experimental results carried on a Permanent Magnet Synchronous Machine which is part of an electro-mechanical actuator designed for an aerospace application. A comparison between the performance of the classical Lumped Parameter Thermal Network and the proposed model is carried out, both in terms of accuracy of the stator temperature prediction and of the computational time required.**

Index Terms—Thermal analysis, electric motors, permanent magnet machines, thermal management, nonlinear dynamical systems, approximation methods, analytical models, polynomials.

I. Introduction

In recent years, the More Electric Aircraft (MEA) initiative has seen significant progress. One of the main areas of interest of the MEA is that of actuation, where electro-mechanical actuators (EMAs) are being proposed as a viable alternative to the traditional hydraulic and electro-hydraulic ones [1]. However, the high requirements in terms of torque density and reliability of these actuating systems still represent a challenge for the system and electrical machine designers.

High performance permanent magnet synchronous machines (PMSMs) coupled to a gearbox and/or a ballscrew is the most common EMA solution, thanks to the high force density of this configuration [2, 3, 4].

PMSMs for EMA applications are often short time or intermittent duty machines (e.g. EMAs for landing gear deployment or for flight control surfaces, respectively). In general this indicates that the machine design is usually more constrained by the magnetic limitations as opposed to the thermal limits [2, 5]. This feature can thus be exploited by increasing the current density in the stator windings so as to improve the overall torque density of the machine [6]. Nevertheless, higher current densities result in large copper losses and higher temperatures, which might shorten the motor life as the windings' electrical insulation would be subject to higher thermal stresses [7].

In order to mitigate this risk, an accurate thermal model is an essential tool for predicting the temperature distribution in the motor. While finite element (FE) and computational fluid dynamics (CFD) thermal models can achieve high resolution, Lumped Parameter Thermal Network (LPTN) models are often preferred thanks to their lower computational effort along with good accuracy [8, 9, 10]. However, the accuracy of any thermal model for electrical machines relies upon a fine tuning of its parameters, due to uncertainties in materials properties, manufacturing tolerances, assembly process, interaction with other drive system components [11, 12].

Thermal models can be used not only at the design stage, but also for the online prediction of the motor temperature distribution [13]. Although LPTNs can provide good temperature estimation [14], their computational cost could still be excessive for online implementation and a trade-off between accuracy and computational speed is necessary [15].

First order LPTNs require less computational effort but are shown to be accurate only for short transients [16]. Methods based on the monitoring of the winding electrical resistance can estimate only the average temperature in the slot [17]. Transfer function approaches as the ones presented for induction machines in [18, 19], allow for computational cost reduction with respect to the LPTNs.

In this paper, a low computational cost (LCC) thermal model for the online prediction of the winding temperature for PMSMs is presented. The model is obtained from a polynomial approximation of the solution of a LPTN. Its computational cost reduction with respect to the original model mainly derives from the fact that the LCC model does not require computation of inverse matrices. Comparing to the

Manuscript received September 8, 2016; Revised October 17, 2016 and January 5, 2017; Accepted January 24, 2017.

C. Sciascera, P. Giangrande, L. Papini, C. Gerada and M. Galea are with the Power Electronics, Machines and Control Group, Department of Electrical and Electronic Engineering, The University of Nottingham, Nottingham, UK (email: eexcs8@nottingham.ac.uk).

original LPTN, the model still shows similar accuracy for different current loads, both during transient and steady state conditions. The proposed model takes into account only the Joule losses, hence it is very well suited for applications where these losses are the main heat source. Indeed, the PMSM investigated herein has high slot current density and relatively low operational speed.

II. Overview of the Proposed LCC Model

The LCC model derives from a simplification of the LPTN. The main feature of the model is that it does not require computation of inverse matrices or of the products between matrices, which is the bottleneck of the LPTN in terms of computational cost.

The procedure for the simplification of the LPTN is reported in detail. In the first instance, the temperature is estimated by means of a 7-node LPTN, which is built by exploiting the motor symmetries. The LPTN is used to estimate the temperature distribution inside a 12-slot/10-pole PMSM. The motor, along with a drawing of its cross-section, is shown in Fig. 1. It is designed for the extension and retraction of a helicopter's landing gear, which can be classified as a short time duty cycle application. The main characteristics of the motor are reported in TABLE I. More details regarding the motor and its overall design procedure can be found in [20].

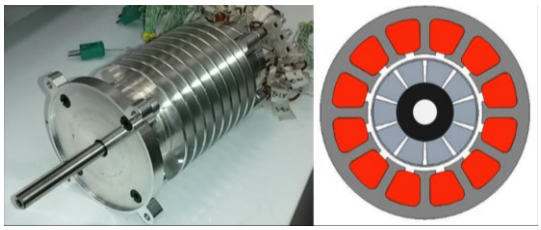

Fig. 1. Picture of the PMSM motor of the EMA for extension/retraction of a helicopter landing gear and its cross-section with no housing.

TABLE I
PMSM MOTOR MAIN PARAMETERS

Parameter	Value	Unit
Nominal current	1	A
Nominal speed	2500	rpm
Power rating	0.3	kW
Stack length	83	Mm
Stator ext. diameter	50	Mm
Rotor ext. diameter	25.5	mm
Airgap thickness	1	mm

Although most of the parameters of the LPTN can be precisely calculated according to the geometry and the physical properties of the materials adopted, there are a number of uncertain parameters, which need to be tuned [21], as the uncertainty of these parameters might compromise the performance of the LPTN. In order to address this, a tuning procedure, based on a Sequential Quadratic Programming (SQP) iterative method for the uncertain parameters of the thermal network has been implemented.

Once the LPTN is properly tuned, a state-space representation of the system is derived for the calculation of an analytical solution for the temperature distribution. The computational cost at this stage of the process is quite high, mainly because the system is time-variant as its state matrix is a function of the current. However, the complexity of the solution can be reduced through a polynomial approximation of the dependency of the system on the phase current.

Following this approximation, the LCC thermal model is then obtained. The model is shown to have very similar accuracy as the original LPTN. Nevertheless, its computational cost is sensibly lower as the model does not require computation of inverse matrices or multiplications between matrices.

A further simplification of the model can be obtained, based on the observation that some of the system dynamics do not contribute significantly to the winding temperature profile. This suggests that the LPTN's number of nodes can be reduced. In this work, a 3-node network was thus derived and validated. Following the same procedure, a lower dimension LCC thermal model was found. Also this model is shown to have similar accuracy compared to the original LPTN.

III. Lumped Parameter Thermal Network

A LPTN models the heat flow and the temperature distribution inside the motor by means of an equivalent thermal circuit, which is composed of heat sources, thermal resistances and thermal capacitances.

In this work, a LPTN is implemented for modelling the heat flow within the PMSM motor, and its schematic is shown in Fig. 2. For symmetry reason only one 12^{th} of the motor is modelled. Due to the low rated speed of the motor, both mechanical and iron losses are neglected. In particular, it was experimentally verified that, respect to the temperature reached when applying an equivalent DC current with a static motor, the increase of temperature due to iron losses is less than 5 °C at the rated speed and rated AC current. Hence, the Joule losses of the windings are the only heat source included in the model. The rotor is simplified as a single element because of the similar thermal properties of the permanent magnets and the back iron which are its main components.

A preliminary selection of the resistances and capacitances can be determined according to the geometry of the motor and from the physical properties of the materials used [22].

The resistances $R_{conv,i}$ represent the heat dissipation by natural convection between the housing external surface and ambient which are calculated as described in (1), where $A_{conv,i}$ represents the contact surface and h_{ext} is the heat transfer coefficient.

$$R_{conv,i} = \frac{1}{A_{conv,i} h_{ext}} \tag{1}$$

Since the heat exchange between stator and rotor through the airgap is assumed to be only by convection, (1) is also used for the calculation of the resistances $R_{ag,i}$ with the airgap heat transfer coefficient h_{ag} in place of h_{ext} and $A_{conv,i}$ a portion of surface of the cylinder whose radius is equal to the median airgap radius. The other resistances represent the heat flows in the motor by conduction. The resistances representing the heat

flow in the radial and in tangential directions are modelled as in (2) and (3), respectively [23]. In (2), r_0 and r_i are the outer and inner radius of the portion of annulus considered, L the stack length of the motor and k the thermal conductivity of the material. In (3), l is the path length of the portion considered and A_{cond} is the conductive surface.

$$R_{radial} = \frac{\ln(r_0/r_i)}{2\pi kL} \tag{2}$$

$$R_{tangential} = \frac{l}{kA_{cond}} \tag{3}$$

The resistance R_{shaft} represents the heat flow through the rotor shaft in the axial direction and it is modelled substituting in (3) half the stack length in place of l and the shaft cross-section area in place of A_{cond}. The capacitances, which model the thermal mass of the respective portion of motor represented, are calculated as the product of mass and specific heat of the material in the considered portion of motor.

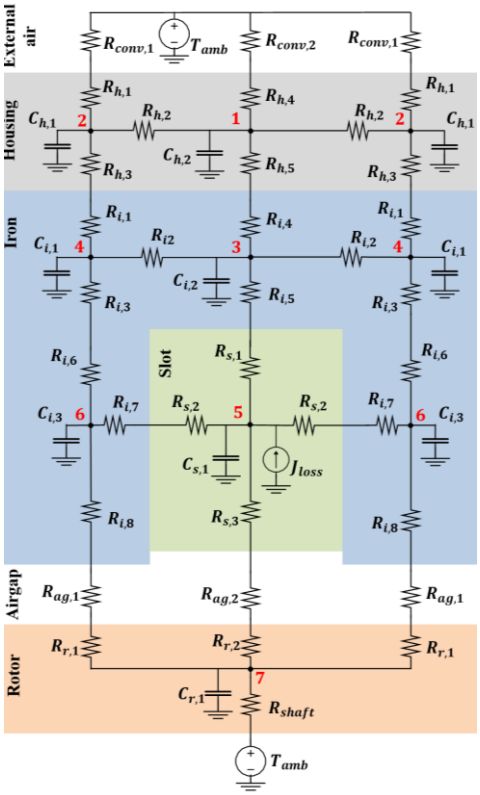

Fig. 2. LPTN representing the heat flow within the motor.

There are some parameters which are not easily determined. Since the motor considered has a random wound winding configuration, the thermal parameters in the slot are uncertain. For this reason, equivalent, aggregate slot thermal conductivity k_{eq} and specific heat capacity c_{eq} values are considered for representing the heat flow through the copper, the electrical insulation and the impregnation of the slot. In particular, the capacitance $C_{s,1}$, which represent the thermal mass of the winding and the impregnation of the slot, is modelled by considering as mass the total mass of the elements in the slot and an equivalent coefficient c_{eq} for the slot specific heat coefficient, which is tuned as explained in the next section.

As shown in [21], the external surface and the airgap convection coefficients are significant parameters, which are not easy to be determined, mainly because of turbulent air flows and orientation of the electrical machine. Further parameters uncertainties are due to the contact resistances which are significantly dependent on the manufacturing tolerances and operating temperatures [24]. Finally, it has to be pointed out that the Joule losses in the slot are temperature dependent, as the electrical resistance of the winding conductor varies with temperature. Therefore, since the winding temperature is not evenly distributed, a correction factor multiplying the Joule losses is introduced in order to account for this.

It can be noticed that some nodes of the circuit of Fig. 2 are equipotential (the ones labelled with the same number) due to circuit symmetries. Thus, the LPTN can be represented by a 7-node equivalent LPTN as the one of Fig. 3. The nodes of the circuit in Fig. 3 are at the same potential of the ones of the circuit in Fig. 2 labelled with the same number. The resistances R_i and the capacitances C_i of the 7-node LPTN can be easily calculated from the computation of the equivalent series and parallel resistances, as well as of the equivalent parallel capacitances of the circuit in Fig. 2.

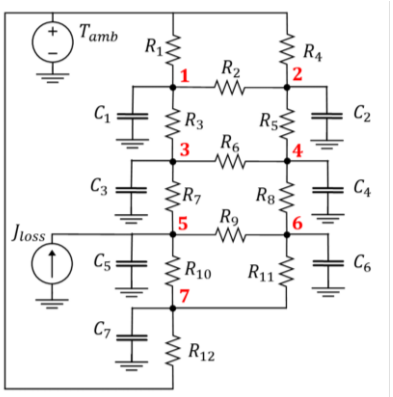

Fig. 3. LPTN equivalent circuit.

A. Critical Parameters tuning procedure

In this section, the LPTN's tuning procedure is presented. The uncertainties on the LPTN's parameters are taken into account by introducing a multiplicative correction factor for each critical parameter. In order to have an accurate estimation of the winding temperature, it is thus sufficient to tune the LPTN's correction factors. This can be achieved by means of a tuning procedure based on experimental results. The procedure can be used to get a LPTN which is very accurate for time varying loads. The first step of the tuning procedure is the determination of the most critical model parameters to be adjusted with a multiplicative correction factor, which are:

- External convection coefficient h_{ext}
- Conductor electrical resistivity R_{el20}
- Lamination thermal conductivity k_{iron}

- Slot equivalent conductivity k_{eq}
- Slot equivalent specific heat capacity c_{eq}
- Housing specific heat capacity c_{hous}
- Airgap convection coefficient h_{ag}

The corrective factors multiplying h_{ext} and h_{ag} account for uncertainties deriving from the heat transfer by convection. The one multiplying R_{el20} tunes the Joule losses. The coefficients k_{eq} and c_{eq} need tuning due to the uncertainty in the heat flow within the slot. c_{hous} is multiplied by a corrective factor because of the uncertainty in the temperature distribution in the housing due to the presence of fins. The corrective factor multiplying the iron thermal conductivity coefficient k_{iron} incorporates the effects of the uncertain thermal resistance of the iron-slot and iron-housing contact surfaces. A general overview of the tuning procedure is as follow:

- Experimental acquisition of winding temperature profiles for different DC currents;
- Definition of an objective function representing the error between LPTN predictions and experimental temperature profiles;
- Use of a Sequential Quadratic Programming (SQP) algorithm that finds a set of optimal correction factors which minimize the objective function.

The slot temperature profiles have been experimentally determined via DC step current tests. During these tests, the motor was placed on a wooden plate in order to reduce the dissipation to ground. The windings were series connected and fed by an EA PSI 8360-15T DC power supply. The winding temperature was measured with 6 K-type thermocouples placed in the core of one slot at different axial positions and acquired with a TC-08 Data Logger at 1 second intervals. The profile with the highest temperatures was the winding temperature profile considered. Another K-type thermocouple was placed at sufficient distance from the motor for measuring the ambient temperature. Each experiment was performed starting with the motor in thermal equilibrium in order to set the initial temperature of the circuit nodes in the model equal to ambient temperature during the tuning procedure.

Since some LPTN's parameters are temperature dependent, several DC current step values (40, 50, 90 and 100% of the rated current) were applied. In this way, the optimizer is "forced" to find a set of parameters which make the LPTN accurate for different loads since the optimization needs to be performed for several specific temperature profiles.

The experimental values are then used as inputs for the optimization problem defined in (4), where *f* is the objective function, the subscript *i* represents the i-th current applied, *t* is the time, $t_{0,i}$ and $t_{f,i}$ are respectively the initial and final time of the temperature profile of the i-th current, whereas $T_{mea,i}$ and $T_{mod,i}$ are respectively the measured and predicted winding temperatures.

$$f = \sum_i err_i$$
$$err_i = \frac{1}{t_{f,i}-t_{0,i}} \left(\int_{t_0}^{t_f} \left(\frac{T_{mea,i}(t)-T_{mod,i}(t)}{T_{mea,i}(t)} \right)^2 dt \right)^{\frac{1}{2}} \quad (4)$$

The SQP iterative method is then implemented in order to find the values of the correction factors which minimize the objective function *f*. The optimization was launched several times, starting from different random correction factors values selected between 0.1 and 10. For most of the initial conditions, the optimization algorithm showed convergence to the same optimum set of correction factors, except for the correction factors of k_{iron} and h_{ag}, which assumed different values for each run of the algorithm. Since these two correction factors scarcely contribute to the general shaping of the winding temperature profiles, then the convergence values selected where those closest to 1. TABLE II shows the reference value of the critical parameters (i.e. correction factors equal to 1) and their adjusted value after calculation of the optimal correction factors. It is important to note that the tuned values of the selected parameters do not actually have a physical meaning as the only objective of the procedure is to minimize the winding temperature prediction error. Only their reference values were determined based on the physical properties of the materials implemented, the motor geometry, and on the base of a preliminary manual tuning. However, their value is not relevant for the tuning procedure, as the correction factors initial values inserted in the algorithm are randomly chosen. TABLE III shows the values of the resistances and capacitances of the 7 node LPTN after the tuning of the critical parameters.

TABLE II
INITIAL AND OPTIMIZED VALUE FOR THE CRITICAL PARAMETERS

Parameter	Reference value	Optimized value	Unit
h_{ext}	40	45.6	[W/(m^2 °C)]
R_{el20}	5.26	5.05	Ω
k_{iron}	29.3	23.7	[W/(m°C)]
k_{eq}	0.1	0.6	[W/(m°C)]
c_{eq}	590	531	[J/(kg °C)]
c_{hous}	897	1166	[J/(kg °C)]
h_{ag}	5	10.5	[W/(m^2 °C)]

TABLE III
TUNED VALUES OF THE RESISTANCES [°C/W] AND CAPACITANCES [J/°C] OF THE 7 NODES THERMAL NETWORK

R_1=23.64	R_7=10.34	C_1=86.79
R_2=0.07	R_8=1.12	C_2=26.42
R_3=0.09	R_9=4.47	C_3=8.37
R_4=77.67	R_{10}=240.29	C_4=2.55
R_5=0.29	R_{11}=747.93	C_5=16.74
R_6=0.48	R_{12}=160.79	C_6=5.49
		C_7=144.32

The LPTN is then used to estimate the winding temperature, but this time considering the optimized values of the critical

parameters, resulting from the above procedure. It is important to highlight that the obtained temperature predictions refer to the hottest spot experimentally detected (and not to the average winding temperature). This is due to the procedure adopted for tuning the network parameters.

In Fig. 4 the estimated winding temperatures (using the corrective factors) are plotted along with the experimental slot temperature profiles. Fig. 4 shows excellent agreement between the experimental (dot lines) and the predicted (continuous lines) slot temperature profiles, for each of the DC current steps tested. In fact, the mean relative error for this wide range of current values is between 0.9% and 1.5%, thus validating the critical parameters tuning procedure.

In order to further validate the model, the LPTN network was then tested for a load cycle where 3 consecutive steps of currents were applied. The current applied, and the measured and the predicted temperatures are shown in Fig. 5. As can be observed excellent similarity is achieved. TABLE IV illustrates the accuracy of the model, where it can be noted that the maximum error obtained over the cycle is only 5.2 °C.

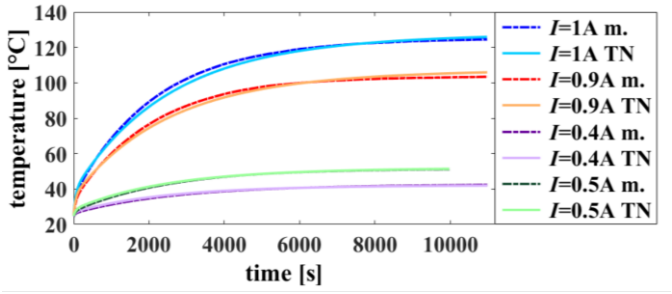

Fig. 4. Measured winding temperatures (m.) compared to the temperatures predicted by the optimized LPTN for current I equal to 40, 50, 90 and 100% of the nominal current.

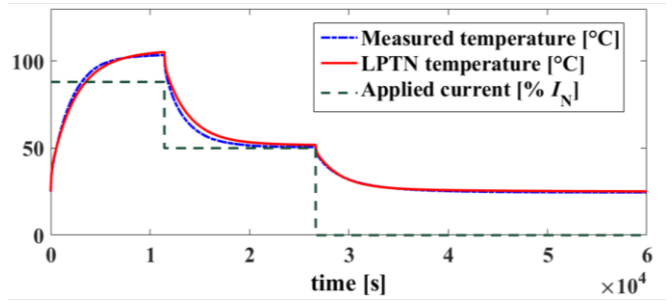

Fig. 5. Measured winding temperature and temperature predicted with the LPTN for three consecutive current steps of 90, 70 and 0% of the nominal current.

TABLE IV
MEAN RELATIVE AND MAXIMUM ABSOLUTE WINDING TEMPERATURE PREDICTION ERROR OF 7 NODES LPTN FOR DIFFERENT CURRENT PROFILES

Load	Mean relative error %	Max. absolute error [°C]
100% I_N	1.5	3.0
90% I_N	1.7	2.5
50% I_N	0.7	1
40% I_N	0.9	0.7
cycle	1.5	5.2

The above results show that very good accuracy can be achieved with the 7-node LPTN for a wide range of operating currents upon careful tuning of some critical parameters. However, the model's computational time needed for the resolution of the equivalent circuit could be excessive for some applications. An analysis of the dynamics involved in the LPTN is reported in the next section, which will lead to the definition of a simplified thermal model characterized by a lower computational cost.

IV. LPTN Analytical Solution

In the previous section, an optimal set of correction factors for the 7-node LPTN was found such that an accurate stator winding temperature estimation could be provided for different current profiles.

Using the well-known node potential method for the resolution of circuits, the LPTN can be represented by the system of first order differential equations described in (5), where T is the vector of the temperatures in the 7 nodes of the thermal network (i.e. vector of the unknowns), u is the inputs vector $[T_{amb}, I^2]^{\mathrm{T}}$ with T_{amb} ambient temperature and I electric current.

$$\dot{T} = AT + Bu \qquad (5)$$
$$A = C^{-1}A_1\,, \qquad B = C^{-1}B_1$$

Matrices A_1, B_1 and C are as shown in (6), where C is a diagonal matrix and A_1 is a symmetric matrix.

$$A_1 = \begin{bmatrix} a_{11} & R_2^{-1} & R_3^{-1} & 0 & 0 & 0 & 0 \\ R_2^{-1} & a_{22} & 0 & R_5^{-1} & 0 & 0 & 0 \\ R_3^{-1} & 0 & a_{33} & R_6^{-1} & R_7^{-1} & 0 & 0 \\ 0 & R_5^{-1} & R_6^{-1} & a_{44} & 0 & R_8^{-1} & 0 \\ 0 & 0 & R_7^{-1} & 0 & a_{55} & R_9^{-1} & R_{10}^{-1} \\ 0 & 0 & 0 & R_8^{-1} & R_9^{-1} & a_{66} & R_{11}^{-1} \\ 0 & 0 & 0 & 0 & R_{10}^{-1} & R_{11}^{-1} & a_{77} \end{bmatrix}$$

$$\begin{aligned} a_{11} &= -(R_1^{-1} + R_2^{-1} + R_3^{-1}) \\ a_{22} &= -(R_2^{-1} + R_4^{-1} + R_5^{-1}) \\ a_{33} &= -(R_3^{-1} + R_6^{-1} + R_7^{-1}) \\ a_{44} &= -(R_5^{-1} + R_6^{-1} + R_8^{-1}) \\ a_{55} &= -(R_7^{-1} + R_9^{-1} + R_{10}^{-1}) + R_{el20} I^2 \alpha_0 \\ a_{66} &= -(R_8^{-1} + R_9^{-1} + R_{11}^{-1}) \\ a_{77} &= -(R_{10}^{-1} + R_{11}^{-1} + R_{12}^{-1}) \end{aligned}$$

$$B_1 = \begin{bmatrix} 0 & R_1^{-1} \\ 0 & R_4^{-1} \\ 0 & 0 \\ 0 & 0 \\ R_{el20}(1 - 20\alpha_0) & 0 \\ 0 & 0 \\ 0 & R_{12}^{-1} \end{bmatrix}$$

$$C = \mathbf{diag}(C_1, \ldots, C_7) \qquad (6)$$

Matrix A_1 is linearly dependent on I^2 through the element a_{55}, since the heat source related to the Joule losses J_{loss} is represented by (7), where R_{el20} and α_0 are physical constants and T_5 is the fifth element of vector T, which represents the temperature in the slot.

$$J_{loss} = R_{el20}\big(1 + \alpha_0(T_5 - 20)\big)I^2 \quad (7)$$

Thus, if the current is not constant, the matrix A_1 will be time-variant.
Under the preliminary hypothesis of constant current *I,* the system is time-invariant, and the general solution of (5) at the generic time t is given by (8), where t_0 is the initial time.

$$T(t) = e^{A(t-t_0)}T(t_0) + \int_{t_0}^{t} e^{A(t-\tau)}Bu\, d\tau \quad (8)$$

Assuming that *A* has 7 distinct eigenvalues (the original LPTN can be designed in order that this assumption is valid), then a linear transformation represented by the orthonormal matrix *M* exists, such that

$$A = M^{-1}\Lambda M, \quad \Lambda = \mathbf{diag}(\lambda_1, \dots, \lambda_7) \quad (9)$$

with λ_i i-th eigenvalue of the matrix *A* and the columns of *M* eigenvectors of *A*. Thus, by considering the change of variables $z = M^{-1}T$, system (5) becomes $\dot{z} = \Lambda z + M^{-1}Bu$, whose solution is given by (10).

$$z(t) = e^{\Lambda(t-t_0)}z(t_0) + \int_{t_0}^{t} e^{\Lambda(t-\tau)}M^{-1}Bu\, d\tau \quad (10)$$
$$e^{\Lambda(t-t_0)} = \mathbf{diag}\big(e^{\lambda_1(t-t_0)}, \dots, e^{\lambda_7(t-t_0)}\big) = K(t)$$

Considering (8), then it can be observed that the exponential matrix in (10) is a diagonal matrix. Therefore, assuming a constant ambient temperature T_{amb}, the integral in (10) can be explicitly calculated and the solution of (5) can be rewritten as in (11). where $S(t)$ is defined in (12).

$$T(t) = MK(t)M^{-1}T(t_0) + MS(t)M^{-1}Bu \quad (11)$$

$$S(t) = \mathbf{diag}\left(-\tfrac{1}{\lambda_1}\big(1 - e^{\lambda_1(t-t_0)}\big), \dots, -\tfrac{1}{\lambda_7}\big(1 - e^{\lambda_7(t-t_0)}\big)\right) \quad (12)$$

Thus, in (11) the temperature profiles in the nodes of the LPTN for the case of constant current *I* are expressed as a linear combination of exponential functions of time *t*.
If a discrete time domain is considered, temperature prediction in case of time-varying current *I* and ambient temperature T_0 can be computed as follows. Defining t_j and t_{j+1} as two consecutive time instants, and assuming the current *I* and the ambient temperature T_0 as constant in the interval $[t_j, t_{j+1})$ and equal to their initial value at time t_j, then by considering (11) with $t_0 = t_j$ and $t = t_{j+1}$, the temperature can be iteratively predicted as shown in (13).

$$\begin{aligned} T(t_{j+1}) &= M(I_j)K(I_j)M^{-1}(I_j)T(t_j) \\ &\quad + M(I_j)S(I_j)M^{-1}(I_j)Bu(T_{0,j}, I_j), \\ I_j &= I(t_j), \qquad T_{0,j} = T_0(t_j) \end{aligned} \quad (13)$$

The assumption of ambient temperature and current constants between two consecutive instants is not critical as the approximation error can be arbitrarily reduced by increasing the sampling time and because the temperature dynamics are typically slow compared to the sampling time of a Digital Signal Processor (DSP).
It has to be noted that in (13) the matrixes *M*, *K* and *S* are functions of the current *I* through the eigenvalues and the eigenvectors of *A*. For this reason, when considering time varying currents, these matrices are to be updated at each instant for a correct calculation of the temperature. Therefore, the computational effort of the temperature prediction could be unsatisfactory. In the next sections a solution for the reduction of the model computational cost will be proposed.

V. Low Computational Cost Model

The computational cost of the analytical solution presented in the previous section is relatively high as the eigenvalues and eigenvectors of *A* need to be calculated at each time instant as well as the inverse of the matrix *M.* In this section, a solution for the reduction of the computational cost of (13) is proposed and investigated. The main steps which lead to the simplified thermal model are the following:

- Calculation of the elements of the matrices in (13) for the current *I* in a specified domain;
- Computation of the 2nd order polynomial approximation of the relationship between the matrices elements and the current *I*;
- Exploitation of the coefficients of the computed polynomial functions for representing each matrix of (13) as 2nd order matrix polynomials of the variable *I;*
- Substitution in (13) of the approximating matrix polynomials for obtaining the simplified model.

As a first step, a maximum current I_{MAX} is fixed and the elements of the matrices *K, S, M* and M^{-1} are calculated for *I* between 0 and I_{MAX}. For the sake of clarity, Fig. 6 shows only the variation of the last four diagonal elements $k_{i,i}, i = 4, \dots, 7$ of the matrix *K* in the range of current considered, normalized to their value at zero current, showing an almost parabolic behavior. However, a similar parabolic behavior can be observed for each of the coefficients of matrix *K*, as well as for each element of matrices *S*, *M* and of its inverse M^{-1}.
The relationship between each element of *K* and the current can be well approximated with a 2nd order polynomial as in (14). The coefficients $c_{Ki,i,n}$ of the approximating polynomial for the i-th element on the diagonal of *K* are calculated using the least squares method.

$$k_{i,i}(I) \cong c_{Ki,i,2}I^2 + c_{Ki,i,1}I + c_{Ki,i,0} \quad (14)$$

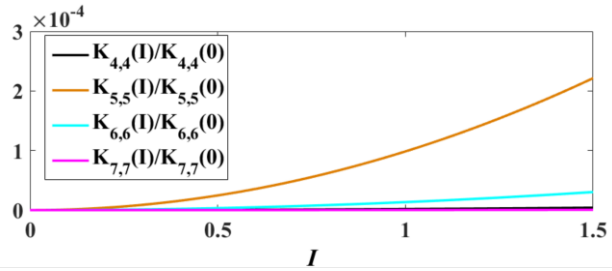

Fig. 6. Last four elements of the diagonal of $\boldsymbol{K}$ respect to current I normalized by their value for I=0.

Similar results were obtained for the relationship of each element of the matrices S, M and of its inverse M^{-1} respect to current I. The same approximating polynomials were therefore used as in (15), where $c_{Si,i,n}$, $c_{Mi,j,n}$, and $c_{-Mi,j,n}$ are the coefficient of the polynomial functions for the i-th diagonal element of S and the i-th row, j-th column of the matrixes M and M^{-1}, respectively.

$$\begin{aligned} s_{i,i}(I) &\cong c_{Si,i,2}I^2 + c_{Si,i,1}I + c_{Si,i,0} \\ m_{i,j}(I) &\cong c_{Mi,j,2}I^2 + c_{Mi,j,1}I + c_{Mi,j,0} \\ m_{i,j}^{-1}(I) &\cong c_{-Mi,j,2}I^2 + c_{-Mi,j,1}I + c_{-Mi,j,0} \end{aligned} \qquad (15)$$

From (14, 15), the matrices K, S, M and M^{-1} can therefore be represented as in (16).

$$\begin{aligned} K &\cong K_2I^2 + K_1I + K_0 \\ S &\cong S_2I^2 + S_1I + S_0 \\ M &\cong M_2I^2 + M_1I + M_0 \\ M^{-1} &\cong \bar{M}_2I^2 + \bar{M}_1I + \bar{M}_0 \end{aligned} \qquad (16)$$

where the elements of the constant matrices at the right side of (16) are the coefficients of the polynomials introduced in (14,15), as summarized in (17), where $k_{n_{i,i}}$, $s_{n_{i,i}}$, $m_{n_{i,j}}$ and $\bar{m}_{n_{i,j}}$ are the elements of K_n, S_n, M_n and $\bar{M}_n$, respectively.

$$\begin{aligned} k_{n_{i,i}} &= c_{Ki,i,n} \\ s_{n_{i,i}} &= c_{Si,i,n} \\ m_{n_{i,j}} &= c_{Mi,j,n} \\ \bar{m}_{n_{i,j}} &= c_{\bar{M}i,j,n} \quad , \quad n = 0,1,2 \end{aligned} \qquad (17)$$

Finally, if the approximations presented in (16) are applied to the matrices of (13), the new LCC model for the temperature prediction is obtained as in (18), where W_i and V_i are constant matrices of dimension 7x7 and 7x2, respectively, that are obtained from the multiplications between the approximating matrices on the right side of (16).

$$T(t_{j+1}) = \sum_{i=0}^{6}\left(W_iI_j^iT(t_j) + V_iI_j^iu(I_j)\right) \qquad (18)$$

Since the matrices involved in (18) are constant matrices which can be calculated once at all, this model significantly decreases the computational cost of the temperature prediction, compared to the LPTN, as at each instant it is not required to compute any matrix inversion or products between matrices.

Although the presented model considers only Joule losses as a heat source, it is important to note that it can be easily extended to applications where the stator iron losses are not negligible. Indeed, with the original LPTN these losses can be modelled as heat sources in the nodes of the stator teeth and the stator yoke [14]. Under the common assumption of temperature independent iron losses, they can be represented as a function of the electrical frequency f and the current I [25]. It follows that the matrix A in (5) is unchanged if the heat sources representing the temperature independent iron losses are included in the original LPTN, and only the input vector u and the input matrix B would be modified. Thus, a procedure similar to the one presented in Sections IV and V can still be adopted for the new system, with the only difference that in (18) the input u will be function of I and f.

In order to validate all the above, the LCC thermal model described by (18) for the fast winding temperature prediction is tested for the same current profiles used in Section III. This also serves to compare the accuracy of the original LPTN to that of the simplified analytical model. In TABLE V the mean relative and the maximum absolute errors of the predicted temperature using (18) respect to the measured slot temperature are reported for each current profile considered. It can be seen that the simplification of the LPTN does not affect sensibly the accuracy of the slot temperature prediction.

TABLE V
MEAN RELATIVE AND MAXIMUM ABSOLUTE WINDING TEMPERATURE PREDICTION ERROR OF ANALYTICAL MODEL FOR DIFFERENT CURRENT PROFILES

Load	Mean relative error %	Max. absolute error [°C]
100% I_N	1.5	2.7
90% I_N	1.6	3
50% I_N	2.2	1.3
40% I_N	2.3	1.3
cycle	1.5	5.2

The model proposed in (18) has similar accuracy as the original LPTN and lower computational cost since it is characterized by reduced complexity. However, its complexity can be further reduced by decreasing the number of nodes of the original LPTN, which would reduce the dimension of the matrices in (18). Thus, in the next section a 3-node LPTN deriving from the original 7-node LPTN is evaluated, from which an even lower computational cost model will be obtained.

VI. LOWER ORDER MODELS

Equations (11, 12) show that the motor temperatures can be represented as linear combination of exponential functions of time t. In particular, the exponents of the exponential functions are in the form $\lambda_i t$, with λ_i i-th eigenvalue of the matrix A. Since in the application considered the magnitudes of these eigenvalues are significantly different, in this section reduced dynamics models are evaluated in order to further reduce the computational cost of the stator temperature prediction.

Assuming that the eigenvalues λ_i of matrix A are ordered such that $\lambda_i < \lambda_j$ for $i < j$, the performance of the reduced dynamics model is investigated by incrementally setting to zero the diagonal elements of matrices K and S in (13). In this way, for instance by setting $k_{1,1}$ and $s_{1,1}$ equal to zero, the exponential functions relative to λ_1 can be neglected.

The reduced models are then tested for each current profile considered in TABLE I. In particular, it was found that, by neglecting the dynamics related to $\lambda_i, i = 1, \dots, 4$ the prediction of the stator temperature is similar to the output of the original LPTN. However, if the dynamics associated to λ_5 are also neglected, then the system accuracy is reduced with a maximum relative error of 22%. This can be observed in Fig. 7, where the stator temperature calculated with the 3rd order ($k_{i,i}$ and $s_{i,i}$ equal to zero for $i = 1, \dots, 4$) and the 2nd order (also $k_{5,5}$ and $s_{5,5}$ equal to zero) models are plotted along with the measured temperature for the current profile of Fig. 5.

It is important to note that the benefits in terms of computational cost of the reduced order models are limited. In fact, setting the appropriate elements of K and S to zero reduces the initial calculation time of the constant matrices of (18), but does not have an impact on the amount of operations to be computed online at each iteration. However, a perceived advantage is that high accuracy could be achieved with a lower order LPTN.

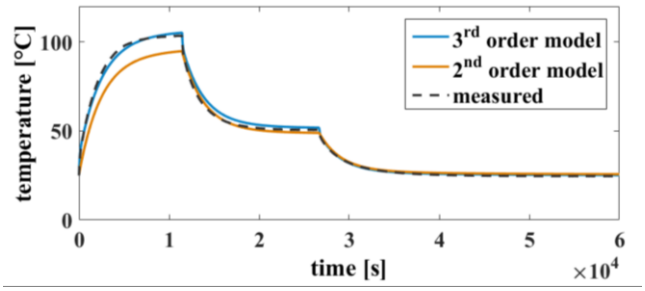

Fig. 7. Measured winding temperature and predicted temperature using second and third order thermal models.

A. Third order model

Considering the above, then the 7-node equivalent circuit of Fig. 3 is reduced to a 3-node circuit by removing its less significant components. For the network of Fig. 3, it can be noticed from TABLE III that the resistances R_2, R_3, R_5, R_6 and R_8, and the thermal masses C_3, C_4 and C_6 are the components with less significance to the overall circuit. In particular, these resistances can be approximated with a short circuit, whereas the capacitances can be discarded. Thus, the 7-node LPTN is reduced to the 3-node LPTN as shown in Fig. 8. The new resistances and thermal masses are defined by (19).

$$R_I = \frac{R_1 R_4}{R_1 + R_4} \qquad R_{II} = \frac{R_7 R_9}{R_7 + R_9}$$

$$R_{III} = \frac{R_{10} R_{11}}{R_{10} + R_{11}} \qquad R_{IV} = R_{12}$$

$$C_I = C_1 + C_2 \qquad C_{II} = C_5 \qquad C_{III} = C_7 \qquad (19)$$

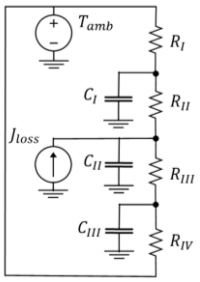

Fig. 8. 3-node LPTN equivalent circuit.

The same procedure described in Sections IV and V can be applied also to the 3-node LPTN introduced. Thus, an analytical model similar to the one of (18) can be obtained also from the new 3-node LPTN, where now T is the vector of the temperatures in the 3 nodes of the LPTN, W_i and V_i are constant matrices of dimension 3x3 and 3x2, respectively, whereas current I_j and input vector u are unchanged. The second element of T represents the temperature in the stator slots. The computational cost of the new model will be lower compared to the one of (18), as shown in TABLE VII, because the dimensions of the matrices involved are more than halved.

B. Validation of the 3rd order model

The reduced computational cost analytical model derived from the 3-node LPTN shown in Fig. 8 is tested for the same experimental current profiles used in Section III.

Fig. 9 shows the measured temperature and the predicted temperature for step currents of 40, 50, 90 and 100% of the nominal current. Fig. 10 shows measured and predicted temperatures for the current cycle introduced in Fig. 5.

In TABLE VI the mean relative and the maximum absolute errors between measured slot temperature and the predicted temperature using the reduced computational cost analytical model are reported for each current profile considered.

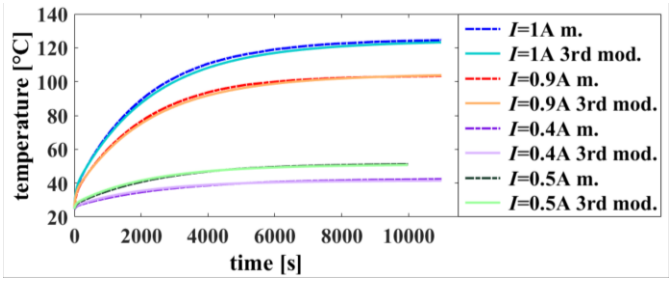

Fig. 9. Measured winding temperatures (m.) compared to the temperatures predicted by the 3rd order analytical model for current I equal to 40, 50, 90 and 100% of the nominal current.

It can be noticed that even in this case the errors are small. In particular, the 3rd order model outperforms the 7-node LPTN in terms of maximum absolute temperature error for the case of the cycle of three step currents. However, as expected the 7-node LPTN has a lower mean relative error, which is the error measure the LPTN was optimized for, as can be seen from the objective function (4).

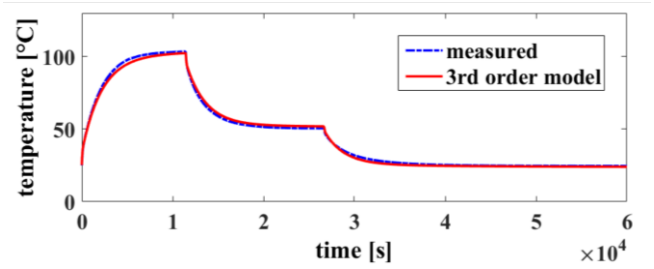

Fig. 10. Measured winding temperature and temperature predicted with the 3rd order analytical model for three consecutive current steps of 90, 70 and 0% of the nominal current.

TABLE VI
MEAN RELATIVE AND MAXIMUM ABSOLUTE WINDING TEMPERATURE PREDICTION ERROR OF REDUCED DIMENSIONS ANALYTICAL MODEL FOR DIFFERENT CURRENT PROFILES

Load	Mean relative error %	Max. absolute error [°C]
100% I_N	2.4	3.3
90% I_N	1.4	2.2
50% I_N	1.4	1.1
40% I_N	1.4	1.1
cycle	2.6	3

Finally, the performance of the 3rd order model has been evaluated considering repeated cycles, in order to take into account the case of intermittent operations. In each cycle, 1A DC was applied for 1000 seconds, followed by 1000 seconds at 0 current. The cycle was repeated 5 times. A comparison between experimental and predicted winding temperatures is shown in Fig. 11, where the maximum absolute error is equal to 2.3 °C.

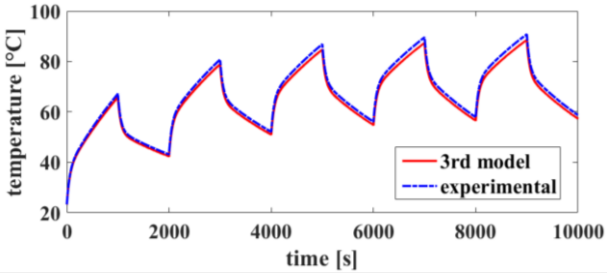

Fig. 11. Measured winding temperatures compared to the temperature predicted by the 3rd order analytical model for repeated cycles, each one composed of 1000 seconds at 1A followed by 1000 seconds at 0A.

C. Computational performance of different methods

A comparative study between the computational speeds of all the models presented above has been done. The models were implemented on MATLAB and run on a standard desktop PC, processor i3-4150 @3.50 GHz, 8GB RAM. The time required at each iteration for the calculation of the winding temperature was recorded using the MATLAB start stopwatcher timer. The results are illustrated in TABLE VII, and show that the simplification of the 7-node LPTN with the 3rd order LCC model allows for an almost 7 times faster computation.

All the above highlights that the analytical solution presented in this paper does give significant advantages in terms of required computational resources without any negative impact on the overall model accuracy.

TABLE VII
COMPUTATIONAL TIME FOR THE TEMPERATURE PREDICTION AT EACH ITERATION FOR THE THERMAL MODELS CONSIDERED

Model	Computational time [10^{-6} s]
7 nodes LPTN	45
3 nodes LPTN	25
7th order LCC model	9
3rd order LCC model	7

VII. Conclusions

In this paper, an innovative, analytical thermal modelling technique for the prediction of electrical machines' winding temperatures has been presented and discussed. As vessel to investigate the proposed method a 12-slot/10-pole PMSM motor was used. The motor's thermal model is derived from a 7-node LPTN. The main feature of the proposed model is its low computational cost respect to the original LPTN, which is achieved through a polynomial approximation of the solution of the LPTN respect to the winding current. Indeed, this is due to the fact that the LCC model does not require computation of inverse matrices or multiplications between matrices. After an evaluation of the system's dynamics, it was observed that a representative 3-node network can be achieved with little impact on the accuracy of the model. Following the same procedure, then from the 3rd order thermal network another even faster analytical model was derived. The inherent velocity and accuracy of this technique would be ideal for its implementation on online temperature prediction platforms, such as are required for aircraft systems' health monitoring and prognostics.

One of the main strengths of this proposed validated technique is its perceived flexibility and applicability to various machine types and families. The authors are already exploring this technique with promising results on similar rating induction machines and synchronous reluctance machines. Another perceived advantage of this technique is its applicability to on-line monitoring of performance. In the future, the authors will be investigating this, by focusing on the implementation of the LCC model on a DSP for online temperature monitoring. A more general version of the model, where also mechanical and iron losses are included, will be also investigated.

References

[1] B. Sarlioglu and C. T. Morris, "More Electric Aircraft: Review, Challenges, and Opportunities for Commercial Transport Aircraft," in *IEEE Transactions on Transportation Electrification*, vol. 1, no. 1, pp. 54-64, June 2015.

[2] M. Galea, C. Gerada, T. Raminosoa and P. Wheeler, "A Thermal Improvement Technique for the Phase Windings of Electrical Machines," in *IEEE Transactions on Industry Applications*, vol. 48, no. 1, pp. 79-87, Jan.-Feb. 2012.

[3] W. Cao, B. C. Mecrow, G. J. Atkinson, J. W. Bennett and D. J. Atkinson, "Overview of Electric Motor Technologies Used for More Electric Aircraft (MEA)," in *IEEE Transactions on Industrial Electronics*, vol. 59, no. 9, pp. 3523-3531, Sept. 2012.

[4] C. Gerada and K. J. Bradley, "Integrated PM Machine Design for an Aircraft EMA," in *IEEE Transactions on Industrial Electronics*, vol. 55, no. 9, pp. 3300-3306, Sept. 2008

[5] T. Raminosoa, C. Gerada and M. Galea, "Design Considerations for a Fault-Tolerant Flux-Switching Permanent-Magnet Machine," in *IEEE Transactions on Industrial Electronics*, vol. 58, no. 7, pp. 2818-2825, July 2011.

[6] M. F. Momen and I. Husain, "Design and performance analysis of a switched reluctance motor for low duty cycle operation," *Industry Applications Conference, 2004. 39th IAS Annual Meeting. Conference Record of the 2004 IEEE*, 2004, pp. 436

[7] C. Sciascera, M. Galea, P. Giangrande, C. Gerada, "Lifetime Consumption and Degradation Analysis of the Winding Insulation of Electrical Machines", *Power Electronics, Machines and Drives (PEMD 2016), 8th IET International Conference on*, Glasgow, 2016, pp. 1-5.

[8] S. Nategh, Z. Huang, A. Krings, O. Wallmark and M. Leksell, "Thermal Modeling of Directly Cooled Electric Machines Using Lumped Parameter and Limited CFD Analysis," in *IEEE Transactions on Energy Conversion*, vol. 28, no. 4, pp. 979-990, Dec. 2013.

[9] C. Kral, A. Haumer and T. Bauml, "Thermal Model and Behavior of a Totally-Enclosed-Water-Cooled Squirrel-Cage Induction Machine for Traction Applications," in *IEEE Transactions on Industrial Electronics*, vol. 55, no. 10, pp. 3555-3565, Oct. 2008.

[10] F. J. Perez-Cebolla, A. Martinez-Iturbe, B. Martín-del-Brío, C. Bernal and A. Bono-Nuez, "Nonlinear Lumped-Circuit Model for Switched Reluctance Motors Exhibiting Core Losses," in *IEEE Transactions on Industrial Electronics*, vol. 63, no. 6, pp. 3433-3445, June 2016.

[11] Boglietti, A. Cavagnino, D. Staton, M. Shanel, M. Mueller and C. Mejuto, "Evolution and Modern Approaches for Thermal Analysis of Electrical Machines," in *IEEE Transactions on Industrial Electronics*, vol. 56, no. 3, pp. 871-882, March 2009.

[12] D. Gerada, A. Mebarki, N. L. Brown, C. Gerada, A. Cavagnino and A. Boglietti, "High-Speed Electrical Machines: Technologies, Trends, and Developments," in *IEEE Transactions on Industrial Electronics*, vol. 61, no. 6, pp. 2946-2959, June 2014.

[13] T. Huber, W. Peters and J. Böcker, "A low-order thermal model for monitoring critical temperatures in permanent magnet synchronous motors," *Power Electronics, Machines and Drives (PEMD 2014), 7th IET International Conference on*, Manchester, 2014, pp. 1-6.

[14] A. Boglietti, A. Cavagnino, M. Lazzari and M. Pastorelli, "A simplified thermal model for variable-speed self-cooled industrial induction motor," in *IEEE Transactions on Industry Applications*, vol. 39, no. 4, pp. 945-952, July-Aug. 2003.

[15] Z. Gao, R. S. Colby, T. G. Habetler and R. G. Harley, "A Model Reduction Perspective on Thermal Models for Induction Machine Overload Relays," in *IEEE Transactions on Industrial Electronics*, vol. 55, no. 10, pp. 3525-3534, Oct. 2008.

[16] A. Boglietti, E. Carpaneto, M. Cossale and S. Vaschetto, "Stator-Winding Thermal Models for Short-Time Thermal Transients: Definition and Validation," in *IEEE Transactions on Industrial Electronics*, vol. 63, no. 5, pp. 2713-2721, May 2016.

[17] M. O. Sonnaillon, G. Bisheimer, C. D. Angelo and G. O. García, "Online Sensorless Induction Motor Temperature Monitoring," in *IEEE Transactions on Energy Conversion*, vol. 25, no. 2, pp. 273-280, June 2010.

[18] N. Jaljal, J. F. Trigeol and P. Lagonotte, "Reduced Thermal Model of an Induction Machine for Real-Time Thermal Monitoring," in *IEEE Transactions on Industrial Electronics*, vol. 55, no. 10, pp. 3535-3542, Oct. 2008.

[19] H. Zhang, "Online Thermal Monitoring Models for Induction Machines," in *IEEE Transactions on Energy Conversion*, vol. 30, no. 4, pp. 1279-1287, Dec. 2015.

[20] C. Sciascera, P. Giangrande, C. Brunson, M. Galea and C. Gerada, "Optimal design of an electro-mechanical actuator for aerospace application," *IECON 2015 - 41st Annual Conference of the IEEE Industrial Electronics Society*, Yokohama, 2015, pp. 001903-001908.

[21] D. Staton, A. Boglietti and A. Cavagnino, "Solving the More Difficult Aspects of Electric Motor Thermal Analysis in Small and Medium Size Industrial Induction Motors," in *IEEE Transactions on Energy Conversion*, vol. 20, no. 3, pp. 620-628, Sept. 2005.

[22] P. H. Mellor, D. Roberts and D. R. Turner, "Lumped parameter thermal model for electrical machines of TEFC design," in *IEE Proceedings B - Electric Power Applications*, vol. 138, no. 5, pp. 205-218, Sept. 1991.

[23] F. Ahmed, E. Ghosh and N. C. Kar, "Transient thermal analysis of a copper rotor induction motor using a lumped parameter temperature network model," *2016 IEEE Transportation Electrification Conference and Expo (ITEC)*, Dearborn, MI, 2016, pp. 1-6.

[24] X. Cai, M. Cheng, S. Zhu and J. Zhang, "Thermal Modeling of Flux-Switching Permanent-Magnet Machines Considering Anisotropic Conductivity and Thermal Contact Resistance," in *IEEE Transactions on Industrial Electronics*, vol. 63, no. 6, pp. 3355-3365, June 2016.

[25] S. Küttler, K. E. K. Benkara, G. Friedrich, F. Vangraefschèpe and A. Abdelli, "Impact of the field weakening on the iron losses in the stator of an internal permanent magnet synchronous machine," *2014 IEEE Energy Conversion Congress and Exposition (ECCE)*, Pittsburgh, PA, 2014, pp. 4188-4195.

Claudio Sciascera received his Bachelor's degree and Master's degree (Hons.) in Mathematical Engineering from the University of Roma "Tor Vergata", Rome, Italy, in 2010 and 2013, respectively. He is now working toward his Ph.D. in electrical and electronic engineering with the PEMC Group, University of Nottingham. His main research interests are lifetime prediction models for electrical machines, thermal management of electrical machines and sensorless control of AC drives.

Paolo Giangrande received his PhD in electrical engineering at the Technical University of Bari in 2011. During 2008, he was a Marie Curie Intra-European Fellow at the University of Malta. Since January 2012, he is a Research Fellow within the PEMC group at the University of Nottingham. His research interests include sensorless control of AC electric drives, as well as design and modeling of electrical machine for aerospace applications.

Luca Papini received his Bachelor degree (Hons.) and Master degree (Hons.) in Electrical engineering in 2009 and 2011, respectively, both from the University of Pisa, Italy. He is currently working towards its Ph.D. with the PEMC Group at University of Nottingham. Since 2013 hold a position of research assistant in the same institution. His main research interests are high speed, high power density electric machines, machine control and levitating system.

Chris Gerada (SM'14) received the Ph.D. degree in numerical modeling of electrical machines from The University of Nottingham, U.K., in 2005. Since 2006, he has been the Project Manager of the GE Aviation Strategic Partnership. In 2008, he was appointed as a Lecturer in electrical machines; in 2011, as an Associate Professor; and in 2013, as a Professor at The University of Nottingham. His research interests include the design and modeling of high-performance electric drives. Prof. Gerada serves as AE for the IEEE Transactions on Industry Applications and as Chair of the IES Electrical Machines Committee.

Michael Galea received his PhD in electrical machines design from the University of Nottingham, UK, where he has also worked as a Research Fellow. He is currently a Lecturer in Electrical Machines and Drives within the PEMC group of the University of Nottingham. He is the Deputy Director of the IAT at the University of Nottingham, where he is also a Lecturer in Aerospace Systems Integration. His main research interests are design, analysis and thermal management of electrical machines and drives.